RESEARCH ARTICLE

TOMOGRAPHY SCHEME FOR 2-QUBIT STATES USING IBM 7-QUBIT OPEN ACCESS QUANTUM PROCESSOR IBMQ_NAIROBI

Talath Humera*[1], B. P. Govindaraja[2], B. G. Divyamani[3], Akshata H Shenoy[4], A. R. Usha Devi[1] and Sudha[2]

[1]Department of Physics, Bangalore University, Jnanabharathi, Bengaluru-560056, India
[2]Department of Physics, Kuvempu University, Shankaraghatta-577451, India
[3]Tunga Mahavidyalaya, Thirthahalli 577432, India
[4]International Centre for Theory of Quantum Technologies, University of Gdánsk, Gdánsk, Poland

ARTICLE INFO	ABSTRACT
	It is well-known that entangled particles have stronger correlations than what is permissible in classical scenario. Entanglement is exploited in the field of quantum computation and quantum technologies. In this era of Noisy Intermediate-Scale Quantum (NISQ) machines one is concerned with tackling *quantum noise* in order to establish their advantage overclassical digital computers. Here we study the performance of IBM open access 7-qubit quantum processor *ibmq_nairobi* for Bell state tomography. We adapt a tomography scheme consisting of 7 measurement operations on the qubits q0, q1 and reconstruct Bell states. We find that there is a marked improvement in our figure-of-merit *quantum fidelity,* after error-mitigation methods are employed.

INTRODUCTION

Quantum computers promise enhanced computational power beyond the realm of classical computing hardware (A. Montanaro, 2016). One of the main hurdles in building scalable quantum hardware is *noise* that can limit their performance. Characterization and control of quantum noise is thus crucial in the development of Noisy Intermediate-Scale Quantum (NISQ) processors (J. Preskill, 2018). Use of present-day noisy quantum computers requires us to ascertain how close are the solutions obtained to the ideal ones. To this end, efforts have been put in towards proof-of-principle tests of various available quantum processors. Cloud quantum computing based on IBM Quantum Platform [3] has made it possible for global users around the world to explore quantum information processing without their own hardware devices. In this work, weemploy the IBM open access 7-qubit quantum processor *ibmq_nairobi* for Bell state tomography.We adapt a tomography scheme consisting of 7 measurements (S. Dogra *et al,* 2021) on the qubits q0, q1 of *ibmq_nairobi* processor and experimentally reconstructthe Bell state density matrices. Organization of our paper is as follows: In Section 2 we give a basic description of quantum state tomography scheme, involving 1 and 2 qubit gates, followed by measurements for reconstructing an arbitrary 2-qubit density matrix. Quantum circuits for the construction of Bell states is also given in this section. Section 3 gives a brief overview of the architecture of the 7-qubit quantum processor *ibmq_nairobi.* Probabilities of measurement outcomes in 5 different trials (with 20,000 shots/trial) of the 7 tomographic operations on *all* 4 input Bell states are subjected to error-mitigation (A. W. R. Smith *et al,* 2021). This is followed by the reconstruction of Bell state density matrices. In Section 4 we evaluate quantum fidelity of input Bell state density matrix with (a) the experimentally reconstructed one & (b) that retrieved after error-mitigation. Section 5 gives a summary of our results.

Quantum Tomography of 2-Qubit State

Qubit Gates and Measurements: A chosen set of 1 qubit gates i.e., Hadamard & X, Y, Z (which are 2×2 Pauli matrices), Rotation gates and 2-qubit Controlled NOT or CNOT gate is employed in quantum computation task. Any arbitrary unitary transformation on *n*-qubit state can be constructed using these single and two-qubit gates (A. Barenco *et al,* 1995). In Table 1 we illustrate the symbols and mathematical representation of qubits, gates and measurements.

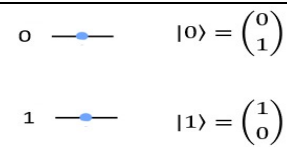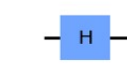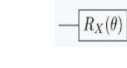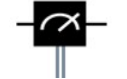**Corresponding Author:* **Talath Humera**
Department of Physics, Bangalore University, Jnanabharathi, Bengaluru-560056, India

Density Matrix of 2-qubit system: A 2-qubit system is characterized by a 4×4 density matrix

$$\rho = \begin{pmatrix} \rho_{00;00} & \rho_{00;01} & \rho_{00;10} & \rho_{00;11} \\ \rho_{01;00} & \rho_{01;01} & \rho_{01;10} & \rho_{01;11} \\ \rho_{10;00} & \rho_{10;01} & \rho_{10;10} & \rho_{10;11} \\ \rho_{11;00} & \rho_{11;01} & \rho_{11;10} & \rho_{11;11} \end{pmatrix} \equiv \begin{pmatrix} \rho_{11} & \rho_{12} & \rho_{13} & \rho_{14} \\ \rho_{21} & \rho_{22} & \rho_{23} & \rho_{24} \\ \rho_{31} & \rho_{32} & \rho_{33} & \rho_{34} \\ \rho_{41} & \rho_{42} & \rho_{43} & \rho_{44} \end{pmatrix}$$

which satisfies the properties (i) Hermiticity: $\rho = \rho^\dagger$ (ii) Unit trace condition: Trρ=1(iii) Positive semi-definiteness: $\rho \geq 0$. These properties lead to $2^4 - 1 = 15$ real independent parameters governing the 2-qubit density matrix.

Table 1. Circuit symbol and associated matrices for qubits, Hadamard, Rotation, CNOT gates and Z measurements.

Circuit symbol & Matrix Representation	
Qubit:	o —●— $\vert 0 \rangle = \begin{pmatrix} 0 \\ 1 \end{pmatrix}$ 1 —●— $\vert 1 \rangle = \begin{pmatrix} 1 \\ 0 \end{pmatrix}$
Hadamard Gate:	—H— $H = \frac{1}{\sqrt{2}} \begin{bmatrix} 1 & 1 \\ 1 & -1 \end{bmatrix}$
Rotation Gate:	$R_X(\theta)$ $R_x(\theta) = \begin{pmatrix} \cos\frac{\theta}{2} & -i\sin\frac{\theta}{2} \\ -i\sin\frac{\theta}{2} & \cos\frac{\theta}{2} \end{pmatrix}$
CNOT Gate:	$\text{CNOT} = \begin{bmatrix} 1 & 0 & 0 & 0 \\ 0 & 1 & 0 & 0 \\ 0 & 0 & 0 & 1 \\ 0 & 0 & 1 & 0 \end{bmatrix}$
Z measurements with outcomes 0, 1	$\Pi_0 = \begin{pmatrix} 1 & 0 \\ 0 & 0 \end{pmatrix}$ $\Pi_1 = \begin{pmatrix} 0 & 0 \\ 0 & 1 \end{pmatrix}$

In order to determine the real independent elements of 2-qubit density matrix the tomography scheme (S. Dogra *et al*, 2021) involving a set of 7 measurements is employed (see Table 2). In particular, explicit evaluation gives $\vec{P}_{zz}=(\rho_{11}, \rho_{22}, \rho_{33}, \rho_{44})^T$, $P_{Hzz}(0,0) - P_{Hzz}(1,0) = 2\text{Re}\rho_{13}$, $P_{Hzz}(0,1) - P_{Hzz}(1,1) = 2\text{Re}\rho_{24}$, $P_{zHz}(0,0) - P_{zHz}(0,1) = 2\text{Re}\rho_{12}$, $P_{zHz}(1,0) - P_{zHz}(1,1) = 2\text{Re}\rho_{34}, P_{zRz}(0,0) - P_{zRz}(0,1) = 2\text{Im}\rho_{12}$, $P_{zRz}(1,0) - P_{zRz}(1,1) = 2\text{Im}\rho_{34}, P_{Rzz}(0,0) - P_{Rzz}(1,0) = 2\text{Im}\rho_{13}$, $P_{Rzz}(0,1) - P_{Rzz}(1,1) = 2\text{Im}\rho_{24}$, $P_{CHzz}(0,0) - P_{CHzz}(1,0) = 2\text{Re}\rho_{14}$, $P_{CHzz}(0,1) - P_{CHzz}(1,1) = 2\text{Re}\rho_{23}$, $P_{CRzz}(0,0) - P_{CRzz}(1,0) = 2\text{Im}\rho_{14}$, , $P_{CRzz}(0,1) - P_{CRzz}(1,1) = 2\text{Im}\rho_{23}$.

Bell States: Bell states $\{\vert\Phi_\pm\rangle = \frac{\vert 00\rangle \pm \vert 11\rangle}{\sqrt{2}}$, $\vert\Psi_\pm\rangle = \frac{\vert 01\rangle \pm \vert 10\rangle}{\sqrt{2}}\}$ form maximally entangled orthogonal & complete set of basis states of the two-qubit Hilbert space. Density matrices of Bell states are given by,
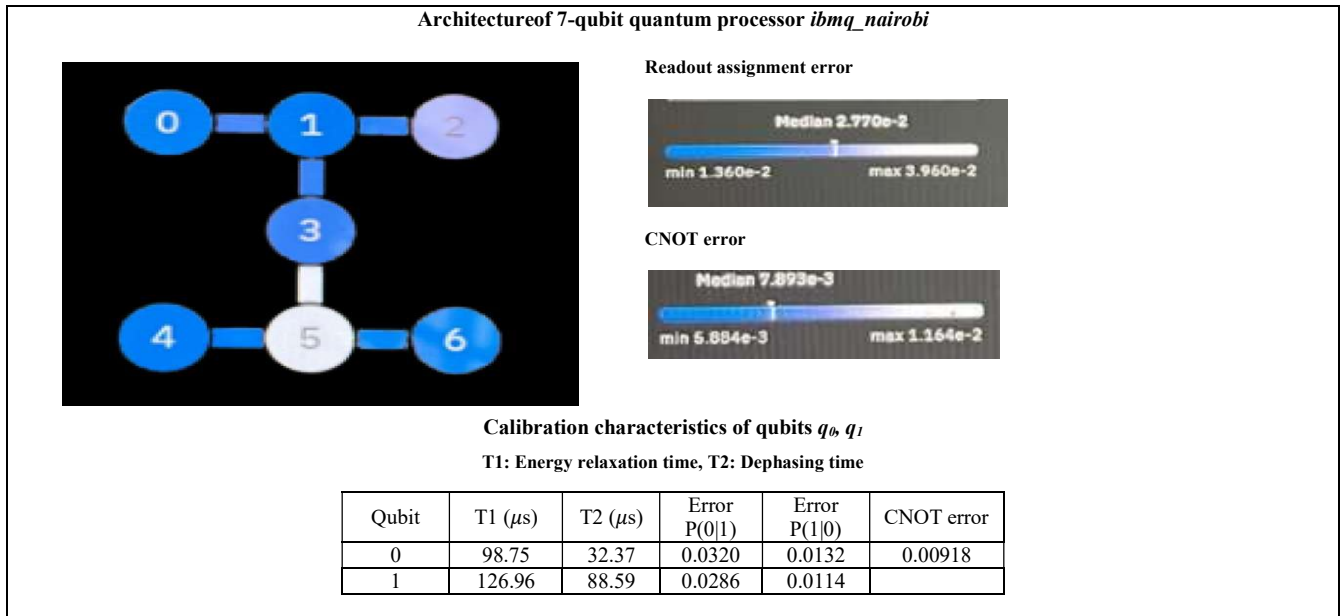
$$\rho_{\Phi_\pm} = \vert\Phi_\pm\rangle\langle\Phi_\pm\vert = \frac{1}{2}\begin{bmatrix} 1 & 0 & 0 & \pm 1 \\ 0 & 0 & 0 & 0 \\ 0 & 0 & 0 & 0 \\ \pm 1 & 0 & 0 & 1 \end{bmatrix}, \rho_{\Psi_\pm} = \vert\Psi_\pm\rangle\langle\Psi_\pm\vert = \frac{1}{2}\begin{bmatrix} 0 & 0 & 0 & 0 \\ 0 & 1 & \pm 1 & 0 \\ 0 & \pm 1 & 1 & 0 \\ 0 & 0 & 0 & 0 \end{bmatrix}$$

Table 2. Quantum tomographic scheme for 2-qubit system

Tomographic operations	Experimental probabilities of z measurements on both the qubits with outcomes $i, j = 0,1$	Elements of ρ
$I \otimes I$	$\vec{P}_{zz} = \{P_{zz}(i,j) = \text{Tr}(\rho\Pi_i \otimes \Pi_j)\}$	$\rho_{11}, \rho_{22}, \rho_{33}, \rho_{44}$
$H \otimes I$	$\vec{P}_{Hzz} = \{P_{Hzz}(i,j) = \text{Tr}(\rho H\Pi_i H \otimes \Pi_j)\}$	Reρ_{13}, Reρ_{24}
$I \otimes R_X(\pi/2)$	$\vec{P}_{zRz} = \{P_{zRz}(i,j) = \text{Tr}(\rho\Pi_i \otimes R_X(\pi/2) \Pi_j R_X{}^\dagger(\pi/2))\}$	Imρ_{12}, Imρ_{34}
$I \otimes H$	$\vec{P}_{zHz} = \{P_{zHz}(i,j) = \text{Tr}(\rho\Pi_i \otimes H \Pi_j H\}$	Reρ_{12}, Reρ_{34}
$R_X(\pi/2) \otimes I$	$\vec{P}_{Rzz} = \{P_{Rzz}(i,j) = \text{Tr}(\rho R_X(\pi/2) \Pi_i R_X{}^\dagger(\pi/2)) \otimes \Pi_j\}$	Imρ_{13}, Imρ_{24}
$(H \otimes I)$ CNOT	$\vec{P}_{CHzz} = \{P_{CHzz}(i,j) = \text{Tr}(\rho\text{CNOT}H \Pi_i H \otimes \Pi_j \text{CNOT}\}$	Reρ_{14}, Reρ_{23}
$(R_X(\pi/2) \otimes I)$ CNOT	$\vec{P}_{CRzz} = \{P_{CHzz}(i,j) = \text{Tr}(\rho\text{CNOT}R_X(\pi/2) \Pi_i R_X{}^\dagger(\pi/2) \otimes \Pi_j \text{CNOT}\}$	Imρ_{14}, Imρ_{23}

Details of the Experiment and Error-Mitigation
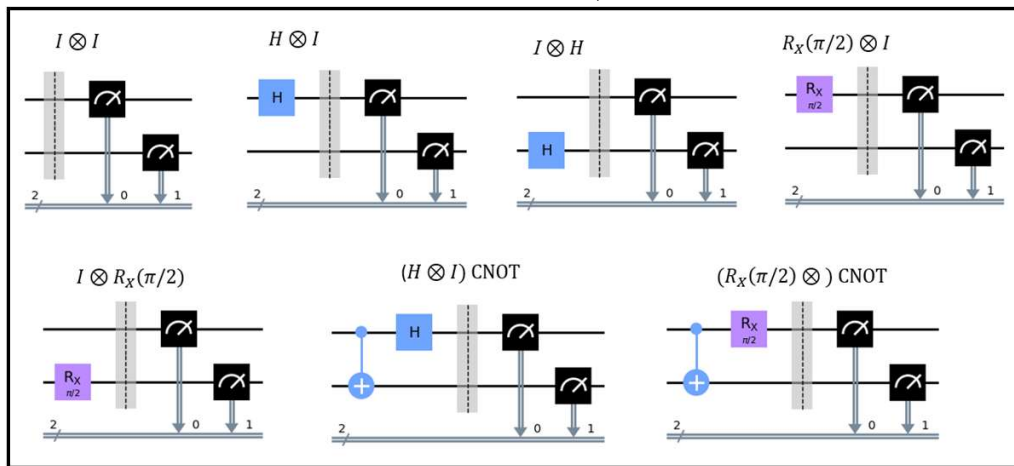
We had open access limited to 10 minutes per month to IBM quantum chips with 7 physical qubits during September 2023. We employed the *zeroth* and *first* qubits q_0, q_1 of IBM 7-qubit processor *ibmq_nairobi* for the experimental creation and tomography of Bell states. Architecture and characteristics of qubits q_0, q_1 of *ibmq_nairobi* is shown in Figure 1.
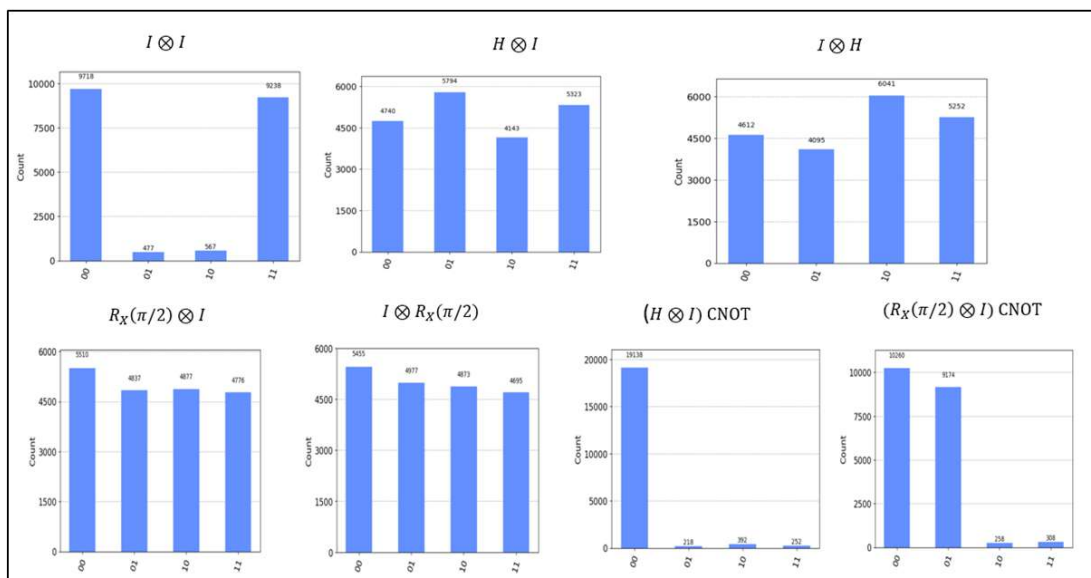
Architectureof 7-qubit quantum processor *ibmq_nairobi*

Readout assignment error

CNOT error

Calibration characteristics of qubits q_0, q_1

T1: Energy relaxation time, T2: Dephasing time

Qubit	T1 (μs)	T2 (μs)	Error P(0|1)	Error P(1|0)	CNOT error
0	98.75	32.37	0.0320	0.0132	0.00918
1	126.96	88.59	0.0286	0.0114	

Figure 1. Architecture and calibration parameters characterizing qubits q0, q1 of the 7-qubit superconducting quantum processor ibmq_nairobi (Credits-IBM)

We created the Bell states $|\Phi_\pm\rangle = \frac{|0,0\rangle \pm |1,1\rangle}{\sqrt{2}}$, $|\Psi_\pm\rangle = \frac{|0,1\rangle \pm |1,0\rangle}{\sqrt{2}}$ and carried out 5 trials with 20,000 number of shots per trial of the 7 tomography operations (see Figure 2 for the quantum circuits corresponding to all 7 tomography operations of Table 2). Experimental counts recorded for theset of 7 to mographic measurements on the Bell state $|\Phi_+\rangle = \frac{|0,0\rangle + |1,1\rangle}{\sqrt{2}}$ in one of thetrials with 20,000 shots is shown in Figure 3.

Figure 2. Quantum circuits for the 7 tomographic operations given in Table 2

Figure 3. Counts recorded in an experimental trial for the 7 tomographic operations on the Bell statestate $|\Phi_+\rangle = \frac{|0,0\rangle + |1,1\rangle}{\sqrt{2}}$. Total number of counts: 20,000.

Quantum error-mitigation: Majorchallenge faced by quantum computers of the NISQ era is to overcome noise. One needs to worry about the *quality* of the qubits in a quantum processor. IBMquantum computers are intrinsically noisy due to imperfect control over their qubits. Quantum error-mitigation (S. Dogra *et al*, 2021 and A. W. R. Smith *et al*, 2021) approach is useful to reduce the effective damage caused by noisy qubits.Consider the experimentally extracted probability vector $\vec{p}_\alpha = \text{Tr}\left(M_\alpha \rho M_\alpha^\dagger\right)$ associated with the outcome $\alpha = 0,1$of measurement operator$M_\alpha$in aqubit state, characterized by the density matrix ρ. One may envisage a possibility of wrongly obtaining the outcome 1 when the qubit is in fact prepared in the state $|0\rangle$. Similarly, it is possible to register the result 0 for the input qubit state $|1\rangle$in a noisy measurement. Corrected probability vector $\vec{p}_{\text{corr}}^{\,(i)} = F_i^{-1}\,\vec{p}^{\,(i)}$ is obtained with the help of the 2×2 calibration matrix $F_i = \begin{pmatrix} f_0^{(i)} & 1-f_1^{(i)} \\ 1-f_0^{(i)} & f_1^{(i)} \end{pmatrix}$, where $f_{0(1)}^{(i)} =$ probability of correctly finding 0 (1) when the i^{th}qubit (which is subjected to measurement process) is in the state 0 (1) and

$1 - f_{0(1)}^{(i)} =$ probability of wrongly obtaining 0 (1) when the ith qubit is in state 0 (1). Corrected two-qubit probability vector isconstructed by using $\vec{p}_{\text{corr}}^{\,(q0,q1)} = F_{q0,q1}^{-1}\,\vec{p}^{\,(q0,q1)}$ where the two-qubit calibration matrix corresponding tomeasurements on two of the qubits q_0, q_1, is given by the 4×4 matrix $F_{q0,q1} = F_{q0} \otimes F_{q1}$. We construct corrected probability vectors $\vec{P}_{zz\,c}$, $\vec{P}_{Hzz\,c}$, $\vec{P}_{zHz\,c}$, $\vec{P}_{Rzz\,c}$, $\vec{P}_{zRz\,c}$, $\vec{P}_{CHzz\,c}$, $\vec{P}_{CRzz\,c}$ from the probability vectors $\vec{P}_{zz}$, $\vec{P}_{Hzz}$, $\vec{P}_{zHz}$, $\vec{P}_{Rzz}$, $\vec{P}_{zRz}$, $\vec{P}_{CHzz}$, $\vec{P}_{CRzz}$ (see Table 2) extracted experimentally. We thus obtain uncorrected experimental density matrices $\rho_{\Phi_\pm}^{(\text{Expt})}$, $\rho_{\Psi_\pm}^{(\text{Expt})}$ as well as the corrected ones $\rho_{\Phi_\pm}^{(\text{Corr})}$, $\rho_{\Psi_\pm}^{(\text{Corr})}$ (retrieved from error-mitigated probabilities) for all the four Bell states.

Quantum fidelity of theoretical and experimentally tomographed bell states before and after error-mitigation

Quantum fidelity of two density matrices ρ and σ, given as $F(\rho,\sigma) = \text{Tr}\left(\rho^{1/2}\,\sigma\,\rho^{1/2}\right)^{1/2}$, is a measure of how close are the two states. We evaluate quantum fidelities (i) $F\left(\rho_{\Phi_\pm}^{(\text{Expt})}, \rho_{\Phi_\pm}\right)$, $F\left(\rho_{\Psi_\pm}^{(\text{Expt})}, \rho_{\Psi_\pm}\right)$ and (ii) $F\left(\rho_{\Phi_\pm}^{(\text{Corr})}, \rho_{\Phi_\pm}\right)$, $F\left(\rho_{\Psi_\pm}^{(\text{Corr})}, \rho_{\Psi_\pm}\right)$ of experimentally reconstructed Bell state density matrices before and after error-mitigation i.e., (i) $\rho_{\Phi_\pm}^{(\text{Expt})}$, $\rho_{\Psi_\pm}^{(\text{Expt})}$ and (ii) $\rho_{\Phi_\pm}^{(\text{Corr})}$, $\rho_{\Psi_\pm}^{(\text{Corr})}$ with theoretical Bell state density matrices$\rho_{\Phi_\pm}$, $\rho_{\Psi_\pm}$. The fidelities before and after error-mitigation for all four Bell states reconstructed from the 5experimental trials are listed in Table 4. Inferring from the Table 4, it is evident that there is a marked improvement in quantum fidelities after error-mitigation.

Summary

We have investigated the performance of IBM open access 7-qubit quantum processor *ibmq_nairobi*for Bell state tomography. Choosing a tomography scheme consisting of 7 measurement operations on the zeroth and first qubits q0, q1 of *ibmq_nairobi*quantum processor we reconstruct the Bell states experimentally. We have used the standard error-mitigation approach to extract corrected experimental probability vectors which in turn determine the corrected Bell state density matrices. It is shown that the *quantum fidelity* gets enhanced significantly after error-mitigation. Our tomographic measurements serve as a proof-of-principle demonstration of the basic processes in a quantum computer.

Table 3. Quantum Fidelities of Bell states before and after error-mitigation

	Bell state $\|\Phi_+\rangle = \frac{\|00\rangle + \|11\rangle}{\sqrt{2}}$			Bell state $\|\Psi_+\rangle = \frac{\|01\rangle + \|10\rangle}{\sqrt{2}}$	
Trial No.	$F\left(\rho_{\Phi_+}^{(\text{Expt})}, \rho_{\Phi_+}\right)$	$F\left(\rho_{\Phi_+}^{(\text{Corr})}, \rho_{\Phi_+}\right)$	Trial No.	$F\left(\rho_{\Phi_+}^{(\text{Expt})}, \rho_{\Phi_+}\right)$	$F\left(\rho_{\Phi_+}^{(\text{Corr})}, \rho_{\Phi_+}\right)$
1	0.93	0.97	1	0.92	0.97
2	0.94	0.97	2	0.93	0.97
3	0.89	0.96	3	0.91	0.96
4	0.96	0.97	4	0.94	0.99
5	0.93	0.99	5	0.93	0.98
	Bell state $\|\Phi_-\rangle = \frac{\|00\rangle - \|11\rangle}{\sqrt{2}}$			Bell state $\|\Psi_-\rangle = \frac{\|01\rangle - \|10\rangle}{\sqrt{2}}$	
Trial No.	$F\left(\rho_{\Phi_-}^{(\text{Expt})}, \rho_{\Phi_-}\right)$	$F\left(\rho_{\Phi_-}^{(\text{Corr})}, \rho_{\Phi_-}\right)$	Trial No.	$F\left(\rho_{\Psi_-}^{(\text{Expt})}, \rho_{\Psi_-}\right)$	$F\left(\rho_{\Psi_-}^{(\text{Corr})}, \rho_{\Psi_-}\right)$
1	0.91	0.96	1	0.89	0.98
2	0.91	0.97	2	0.92	0.98
3	0.88	0.95	3	0.88	0.96
4	0.92	0.98	4	0.91	0.98
5	0.92	0.98	5	0.90	0.98

REFERENCES

A. Montanaro, *Quantum algorithms: An overview*, npj Quantum Inf. 2, 15023 (2016)

J. Preskill, *Quantum Computing in the NISQ era and beyond*, Quantum, 2, 79, (2018)

IBM quantum computing platform https://quantum-computing.ibm.com/

S. Dogra, A. A. Melnikov, G. S. Paraoanu, *Quantum simulation of parity–time symmetry breaking with a superconducting quantum processor*, Comm. Phys. 4, *26* (2021)

A. W. R. Smith, K. E. Khosla, C. N. Self, M. S. Kim, *Qubit readout error mitigation with bit-flip averaging,* Sci. Adv. 7, eabi8009 (2021)

A. Barenco, C. H. Bennett, R. Cleve, D. P. DiVincenzo, N. Margolus, P. Shor, T. Sleator, J. A. Smolin, H. Weinfurter, Elementary gates for quantum computation, Phys. Rev. A 52, 3457 (1995)

****